Molecular statics simulation of CdTe grain boundary structures and energetics using a bond-order potential

OPEN ACCESS
IOP Publishing
Modelling and Simulation in Materials Science and Engineering
Modelling Simul. Mater. Sci. Eng. **26** (2018) 045009 (15pp) https://doi.org/10.1088/1361-651X/aaba87

Molecular statics simulation of CdTe grain boundary structures and energetics using a bond-order potential

Guillaume Stechmann, Stefan Zaefferer and Dierk Raabe

Max-Planck-Institut für Eisenforschung GmbH, Max-Planck-Straße 1, D-40237 Düsseldorf, Germany

E-mail: g.stechmann@mpie.de

Received 9 January 2018, revised 23 March 2018
Accepted for publication 29 March 2018
Published 20 April 2018

Abstract

The structure and energetics of coincidence site lattice grain boundaries (GB) in CdTe are investigated by mean of molecular statics simulations, using the Cd–Zn–Te bond-order potential (second iteration) developed by Ward *et al* (2012 *Phys. Rev.* B **86** 245203; 2013 *J. Mol. Modelling* **19** 5469–77). The effects of misorientation (Σ value) and interface plane are treated separately, complying with the critical need for full five-parameter characterization of GB. In addition, stoichiometric shifts, occurring between the inner interfaces and their adjacent atomic layers, are also predicted, revealing the energetic preference of Te-rich boundaries, opening opportunities for crystallography-based intrinsic interface doping. Our results also suggest that the intuitive assumption that $\Sigma 3$ boundaries with low-indexed planes are more energetically favorable is often unfounded, except for coherent twins developing on {111} boundary planes. Therefore, $\Sigma 5$, 7 or 9 boundaries, with lower interface energy than that of twin boundaries lying on different facets, are frequently encountered.

Keywords: CdTe, grain boundary, molecular statics

(Some figures may appear in colour only in the online journal)

Introduction

During the past decade, cadmium telluride (CdTe) solar cells made the transition from an originally promising material into a real and mature commercial technology. Record laboratory cell efficiencies are still increasing, reaching 22.1% in 2016 [1], whereas full size modules overpassed 18%. Nevertheless, a lot of performance improvement paths can still be explored, one of them being in the direction of the open circuit voltage. Recently, the 1 V barrier has been overcome in doped single crystals [2]. This value remains, however, relatively low when compared to the CdTe bandgap (1.5 eV). This is mostly due to the low carrier concentrations achievable in the absorber layer, resulting from the difficult doping of CdTe, and due to parasitic recombinations of the photo-generated carriers. The tight link existing between carrier density and crystallographic defects emphasizes the crucial role of the latter on cell performance. In particular, grain boundaries (GB) have been proven to significantly alter the charge transport in CdTe layers [3–5], although their actual effects remain equivocal. It is likely that a better understanding of their structure and formation mechanisms will help uncovering their role in this context.

Molecular dynamics and molecular statics (MS) simulations are pertinent tools to resolve the structural and energetic properties of defects, as well as to capture the growth features of thin films. The accuracy of such simulations relies on a careful parameterization of the considered atomistic potentials and an adequate choice of the probed time scales. In the case of CdTe, Ward and Zhou conducted detailed studies in this direction [6–8] and developed a bond-order potential (BOP) that has been found to yield particularly accurate results in term of vapor deposition [8] and defect energy trends, such as dislocation line energies [9], or vacancy and interstitial energies [7]. BOPs encompass a wider range of analytic interatomic potentials which adopt Pauling's [10] and Coulson's [11] bond-order concept. This means that they express the binding energy of a system as a sum over all atomic pairs considering a so called bond-order term which is a function of the local environment of an atom [12–14]. Using such a bond-order term introduces the advantage over conventional interatomic force field formulations in that they are capable of describing different bonding states of an atom which allows them to access chemical reactions and to include effects associated with directional, topological and energetic bond anisotropy.

The development of BOPs for the CdTe system marks a major breakthrough, enabling to conduct meaningful atomistic simulations without the need for computationally very costly *ab-initio*, i.e. density functional theory (DFT), calculations. BOPs thus allow performing static and dynamic simulations involving large numbers of atoms. In the present work, these CdTe BOP potentials are employed to model the structure of a specific set of coincidence site lattice (CSL) GB, which were experimentally observed in CdTe layers [15], at the atomic scale.

MS simulation setup and parametrization

MS simulations were performed using the LAMMPS package [16] and the Cd–Zn–Te potential (second iteration) developed by Ward *et al* [6, 17]. The Ovito software [18] was used for visualizing the simulation results and for first order analysis of the data.

GB structures were created by successive relaxations of two adjoining crystallites, with controlled orientations. In every case, the total number of atoms included in the simulation was in the order of $\sim 5 \times 10^4$. The rotational parameters of the interface, that is, boundary misorientation and interface planes, were thus initially defined, whereas the energy

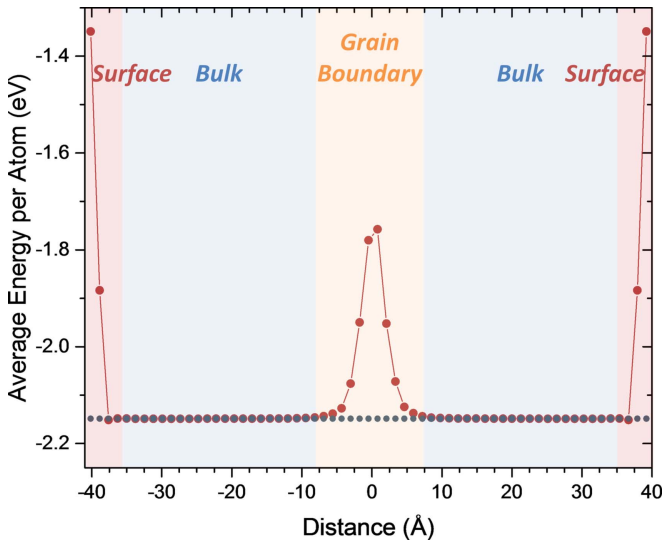

Figure 1. Average energy per atom as a function of the position perpendicular to the both the GB and free surfaces. Red dots correspond to a system, here taken as a case study, composed of a $\Sigma 3\{110\}||\{110\}$ boundary at position $x = 0$ and of two free $\{110\}$ surfaces at both edges. Blue dots correspond to a single crystal.

minimization step was in charge of relaxing the translational parameters. In order to probe the complete energy space, and not only one specific local energy minimum, the translational parameters were actually pre-constrained prior to each relaxation step. This was performed by additionally translating one side of the boundary into a plane parallel to the interface. Therefore, one relaxed structure was created as output per translation vector. The energy minimization step was done in two steps, comprising a standard energy relaxation procedure, by adjusting atom coordinates, combined with a relaxation of the simulation box to release the stress accumulating in the periodic directions. Periodic boundary conditions were only enforced in the directions coplanar with the interface, thus creating a free surface standing opposite to the GB. This prevents interatomic stresses from building up in this direction and circumvents the issue of GB polarity reversal, which would have had otherwise occurred along this direction. Both crystals were created large enough so that this free surface does not affect the GB energetics. This was confirmed by verifying that the atomic potential energy reaches a plateau after the first $\approx$10–20 Å away from the surface, thus mimicking a bulk value, as visible in figure 1 and as will be later discussed in greater detail.

The polarity issue originates from the fact that CdTe crystallizes in the non-centrosymmetric $F\bar{4}3m$ space group. This leads, for example, to the existence of two chemically distinct (111) and $(\bar{1}\bar{1}\bar{1})$ planes, the former being exclusively composed of Cd atoms, whereas the latter has a monoatomic Te composition. As a result, the $\{111\}$ plane family is said to be *polar*. Therefore, for a given set of rotational parameters, the initial number of atomic configurations to be considered before relaxation strongly depends on the polarity of the boundary planes, as emphasized in table 1. Coupling the possible starting configurations, summarized in table 1 and the atomic translation grid used for relaxation, resulted in up to around 800 different starting configurations which were relaxed for every set of rotational parameters. In the following, the reported quantitative values were arbitrarily averaged over the ten configurations with the lowest energies. Since the function minimizing the energy of

Table 1. Number of possible unrelaxed variants of atomically sharp {hkl}||{hkl} and {hkl}||{h′k′l′} interfaces, for a given misorientation, depending on the initial polarities of {hkl} and {h′k′l′} planes.

	{hkl} apolar	{hkl} polar
{h′k′l′} apolar	4	8
{h′k′l′} polar	8	16
{hkl} apolar	3	—
{hkl} polar	—	10

Table 2. Atomic number density ρ' of CdTe bulk crystallographic planes with a lattice constant of 6.478 Å. Apolar planes appear in red, whereas polar ones are marked in blue.

Plane	ρ' (u.d.)
{110}	1.12
{111}	0.91
{100}	0.79
{112}	0.65
{114}	0.37
{120}	0.35
{115}	0.30
{122}	0.26
{017}	0.22
{127}	0.22
{255}	0.22
{034}	0.16

different starting configurations is surjective, that is, different initial structures can output similar relaxed boundaries, the reported standard deviations can be zero in the case where all of these ten configurations are identical.

In order to extract quantitative information from the GB region, it is necessary to provide a clear definition of the interface at the atomic level. In the present work, the differentiation between bulk and GB atoms was established based on their coordination geometry. This was performed by adopting the diamond structure identifier available in the OVITO code [18], derived from the conventional common neighbor analysis method, and described in [19]. As such, all particles having at least a first or a second neighbor not positioned on a zincblende lattice site were assigned to the GB. Based on this distinction, three different parameters, namely the GB energy γ, boundary stoichiometry σ, and boundary atomic density ρ were attributed to each interface. The first one, γ, quantifies the extra energy of the interface, relative to the bulk. It is usually obtained by comparing the energy of a system containing a GB, with the energy of a bulk single crystal. However, in the case of zincblende structures, the issue of polarity inversion prevents the use of periodic boundary conditions in the direction perpendicular to the interface, as aforementioned. Therefore, only the energy of the GB plus the energy of the free surfaces thus formed can be directly obtained. As such, it is important to evaluate the contribution of the free surfaces to the relaxed system energy. The energy profiles of a system containing a GB and two free surfaces, on the one hand, and of a single crystal, on the other hand, are displayed in figure 1, in the direction perpendicular to the

interfaces. It clearly appears that the long range elastic contributions of the free surfaces are negligible, and only affect the first ~5 Å next to the crystal edges. The effect of the GB itself is, however, much more pronounced, and covers around 20 Å. In between these interfaces, the average energy per atom has a constant 'bulk' value, which is found to be the same as what is obtained in a single crystal simulation. The GB energy γ can thus be obtained in a conventional way by comparing the energy of the system encompassing the GB, but excluding the first atomic layers next to the surfaces, with an identical volume in a single crystal. Normalizing this value by the interface area provides a GB energy in $J\,m^{-2}$.

Since distorted bonds and deviations from the zincblende coordination strongly affect the electronic band structure of semiconductors, the atomic number density of the boundary ρ is introduced. It quantifies the *absolute* number of boundary atoms, normalized by the interface area. This leads to values of ρ in units of $mol\,m^{-2}$ (for the sake of convenience, most of the results are actually given in unit of density, u.d., with 1 u.d. being equal to $10^{-5}\,mol\,m^{-2}$). It may be useful to also introduce a *relative* indicator, i.e. a parameter quantifying only the excess number density of distorted atoms, as compared to the initial atomic density of the crystallographic plane composing the boundary. To this end, the dimensionless variable P is introduced and defined as follows in equation (1):

$$P = \frac{\rho}{\rho_A{}' + \rho_B{}'} \tag{1}$$

with ρ the atomic number density of the relaxed boundary, as-defined above, and $\rho_A{}'$, respectively $\rho_B{}'$, the density of the atomically sharp A, respectively B, crystallographic planes forming the $\Sigma X\,A||B$ interface. The use of the ρ' denomination is employed to stress that these values correspond to non-relaxed structures, whereas ρ requires an energy minimization step. Therefore, P can be envisaged as a measure of the sharpness of the relaxed interface, where higher values of P indicate boundaries extending over several parallel atomic planes. Moreover, the critical case, namely, when P equals 1, corresponds to GB formed by pure juxtaposition of bulk crystals with minimum relaxation needed. The atomic number densities of low-indexed boundary planes of the cubic sphalerite space group are tabulated in table 2.

Finally, the boundary stoichiometry σ measures the Cd/Te atomic ratio in the distorted area. It is, therefore, a dimensionless variable. It should be noted that, although a stoichiometric shift can be observed in the boundary, it is in any case compensated by an opposite enrichment/depletion in the boundary surroundings, since the overall structures have a perfect one to one Cd/Te ratio. As such, σ only measures the chemical variation between the inner interface and its vicinity.

Even though GB are not planar defects, but rather have an associated defective volume, values are normalized by the interface area to compare simulation data with experimental measurements.

Results and discussion

Σ3 interfaces

Due to the remarkably low stacking fault energy of CdTe of around $9\,mJ\,m^{-2}$ [20], a significant fraction of GB observed in these layers are Σ3 twin boundaries, namely, around 60% of the total interface network length [15]. The Σ value refers to the reciprocal fraction of coinciding atomic sites in the superlattice formed by the two adjoining crystallites with respect to all atoms in the lattice. Therefore, GB exhibiting this misorientation relationship, thereby defining three out of five rotational parameters, are expected to be composed of small

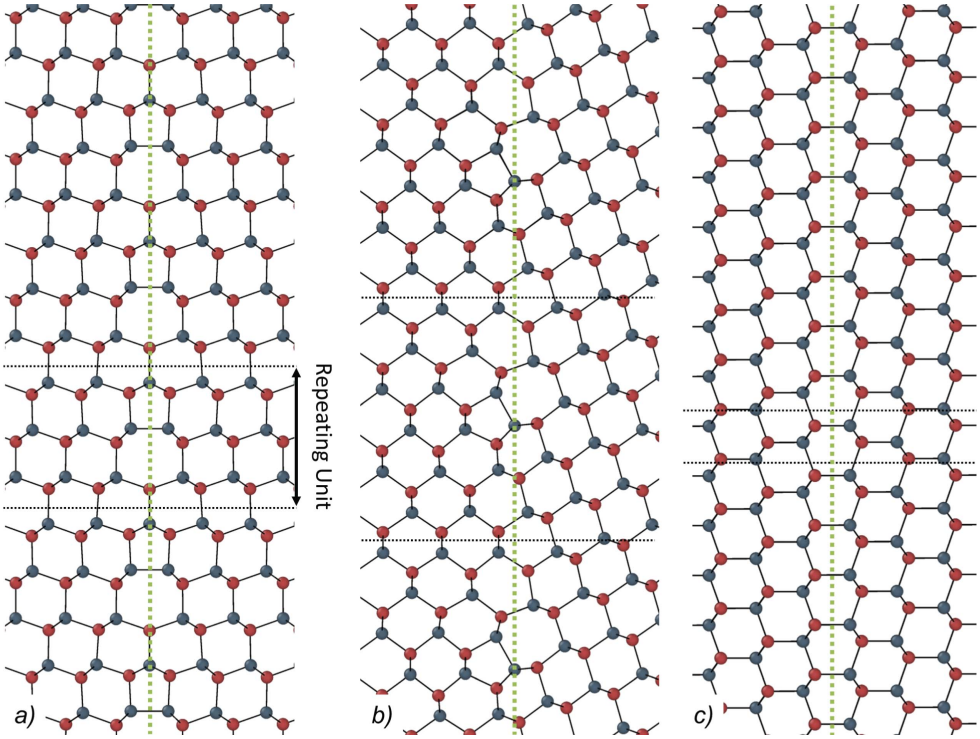

Figure 2. Σ3 GB relaxed structures emphasizing the interface periodicity. (a) {112}||{112}, (b) {110}||{114}, (c) {111}||{111}. Cadmium atoms appear red whereas tellurium atoms are displayed in blue. Note that bonds are arbitrarily drawn, based on the distance between nuclei, and not based on actual electronic interactions between atoms.

repeating units when the interface plane is straight, reflecting the periodicity of the CSL. This is indeed what is observed after energy minimization, as visible in figure 2. In this figure, three different relaxed Σ3 twin boundaries, all exhibiting periodic units in the order of few cubic nanometers, are displayed. The structures presented in this figure correspond to the lowest energy configurations, extracted among all possible combinations of starting polarity and atomic translations as aforementioned.

Quantitative data obtained on a broader variety of Σ3 boundaries are presented in figure 3. As can be observed, the energy of the coherent Σ3{111}||{111} interface calculated with the BOP is almost zero. This is due the tendency of the potential to underestimate the stacking fault energy of CdTe as already reported by Zhou *et al* [9]. The energy of coherent twin boundaries can be generally well approximated by taking half of the stacking fault energy, leading to an expected value of around $5 \times 10^{-3}\,\mathrm{J\,m^{-2}}$. This is, in any case, well below the values calculated for any other boundary planes. The reported data are hardly comparable with other studies, as there is a lack of publications dealing with GB energy calculations in the CdTe literature. One of the only incoherent Σ3 boundaries, being extensively studied, is the {112}||{112} boundary. In this work, the calculated energy of this interface is around $0.53\,\mathrm{J\,m^{-2}}$ which is slightly lower, but still in good agreement, with the value of $0.6\,\mathrm{J\,m^{-2}}$ reported by Park *et al* [21] from first-principle DFT calculations.

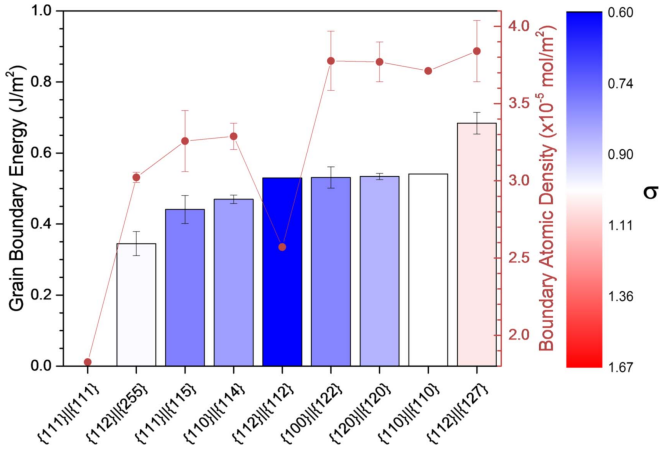

Figure 3. GB energies γ and atomic number densities ρ of several relaxed $\Sigma 3$ twin boundaries, lying on different atomic planes. Bars are color coded accounting for the stoichiometry σ of the interface, expressed in Cd:Te ratio. GB are ordered with increasing γ value.

Table 3. Absolute (ρ) and relative (P) atomic number densities of the $\Sigma 3$ boundaries set displayed in figure 3.

$\Sigma 3$ facet	ρ (u.d.)	P
{111}||{111}	1.83	1.00
{110}||{110}	3.71	1.66
{112}||{112}	2.57	1.99
{110}||{114}	3.29	2.20
{111}||{115}	3.26	2.67
{100}||{122}	3.78	2.73
{112}||{255}	3.02	3.51
{112}||{127}	3.80	4.41
{120}||{120}	3.72	5.31

Furthermore, both, the present study and the work of Park *et al* [21] emphasize the lowest energy of the Te-rich boundary, supporting the numerical values reported in this work.

A general trend observed in figure 3 corresponds to the increase of the interface energy γ with the boundary atomic number density ρ. One exception nevertheless arises in the case of the $\Sigma 3\{112\}||\{112\}$ boundary, where the calculated atomic number density is dramatically lower than for other interfaces with similar energy. It is likely that the crystallographic symmetry of the boundary planes plays a significant role here. The influence of symmetry appears more clearly when correcting for the initial density of the planes involved in the boundary as displayed in table 3. As expected, the P value of the coherent $\Sigma 3\{111\}||\{111\}$ boundary is equal to 1, since the interface is formed by simple juxtaposition of sharp {111} atomic planes. In addition, symmetric $\Sigma 3$ boundaries tend to exhibit the lowest relative densities, implying a higher interface sharpness.

As visible in figure 3, the lowest energy configuration is actually obtained for the $\Sigma 3\{112\}||\{255\}$ interface. This result supports the previous observation, namely, that

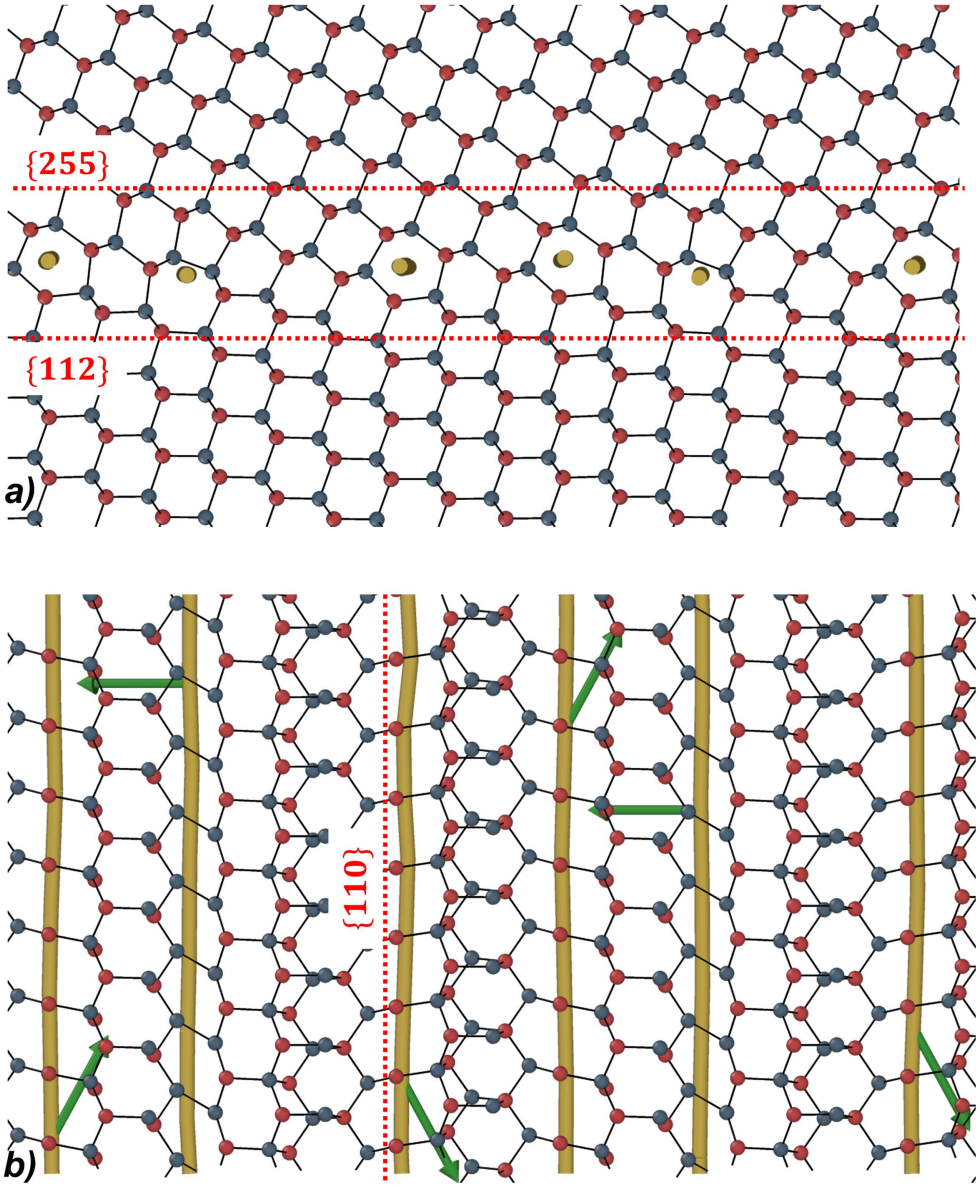

Figure 4. Relaxed $\Sigma 3\{112\}||\{225\}$ GB. (a) Display perpendicular to the boundary plane, yellow features indicate boundary dislocation lines pointing perpendicular to the figure. Red dashed lines indicate plane traces. (b) Rotated view in the boundary plane, displaying the periodic dislocations arrangement of GB dislocations. Green arrows indicate the direction of the Burgers vectors. All dislocations are Shockley partials, with a $1/6\langle 112\rangle$ Burgers vector.

low-indexed planes and symmetric interfaces do not necessarily lead to the lowest boundary energy. The atomic structure of this GB is displayed in figure 4 and is found to be composed of three sets of Shockley partial dislocations, with $1/6\langle 112\rangle$ Burgers vector. These dislocations share a common $\langle 110\rangle$ line direction in both grains and are of the edge (1 set) and 30°

mixed (2 sets) types. Interestingly, this dislocation arrangement is the only one that can be resolved by the dislocation analyzer available in the Ovito software [18, 22]. In this case, the GB is recognized as a well-ordered structure across which Burgers circuits can be easily mapped. In contrast, for all other boundaries the software returns a 'non-crystalline' area, which is clearly more disordered. The higher order of the former boundary results in a lower energy of this one compared to all others.

In figure 3, bars are color coded accounting for the stoichiometry of the boundary. It is apparent that for most of the incoherent twin boundaries studied, lowest energy configurations are either Te-rich (σ lower than 1) or stoichiometric (σ equals to 1). The only exception is the $\Sigma3\{112\}\{127\}$ interface, which is slightly Cd-rich. Since all different possible starting configurations had been tested, it is possible to compare the different features among similar boundaries with reversed chemical composition. The main difference between Cd and Te lies in their electronic configurations. While Cd possesses two valence electrons, Te has six. Therefore, while two doubly-bonded Cd atoms will repel each other due to the Coulomb interaction of their nuclei, the same is mitigated in the case of Te, due to the possible electronic interactions between their remaining valence electrons. This trend seems to be particularly well-captured in the BOP and it explains quite well the energy difference between the Te- or Cd-rich $\Sigma3\{112\}\{122\}$ interface as reported in this work ($\Delta\gamma = 0.2\,\mathrm{J\,m^{-2}}$) and also observed by Park *et al* [21] ($\Delta\gamma = 0.1\,\mathrm{J\,m^{-2}}$). The structure of the Te-rich $\Sigma3\{112\}\{112\}$ GB is displayed in figure 2(a). Another example of the critical role of stoichiometry on the boundary energy is visible in the case of $\Sigma3\{111\}\{115\}$ GB as displayed in figure 5. Since both boundary planes are polar, four different chemical variants of the same structure exist. It appears once again that Te-rich cores exhibit the lower energies, whereas higher Cd concentration in the core leads to higher σ values. As can be observed in figure 5, the σ value does not fully capture this chemical trend, as it averages the Cd/Te ratio over the full thickness of the boundary. Therefore, it distinguishes between bulk and boundary, rather than between GB core and GB outermost. The larger thermodynamic stability of Te-rich boundaries may be a beneficial factor for CdTe as Zhang *et al* [23] pointed out that these interfaces are more likely to be efficiently passivated upon chlorine annealing.

When comparing the properties of the atomically sharp GB (plane polarity, ρ') with their relaxed counterparts (σ, ρ), it appears that no prediction can be easily made *a priori*, solely based on the features observed on unrelaxed interfaces. This is clearly emphasized by the overall large P values reported in table 3.

Higher-order Σ interfaces

The study of CSL boundaries becomes increasingly complex with increasing values of Σ. Indeed, as mentioned in the previous section, the volume of the CSL unit cell linearly scales with the Σ value. As such, if the boundary planes are kept identical, a $\Sigma9$ boundary would require a simulated volume cell three times larger than its $\Sigma3$ counterpart, to keep the simulated CSL period number constant. As a result, computation times severely increase and only few high-order Σ boundaries with low-indexed boundary planes can technically be studied.

Second order $\Sigma9$ twin boundaries. In materials with a low stacking-fault energy, $\Sigma9$ interfaces usually represent a non-negligible fraction of the total GB network length (commonly around one-fifth of the $\Sigma3$ fraction [15, 24]). This is due to the fact that their density is enforced by successive twinning between adjacent grains according to the CSL multiplication rule [24].

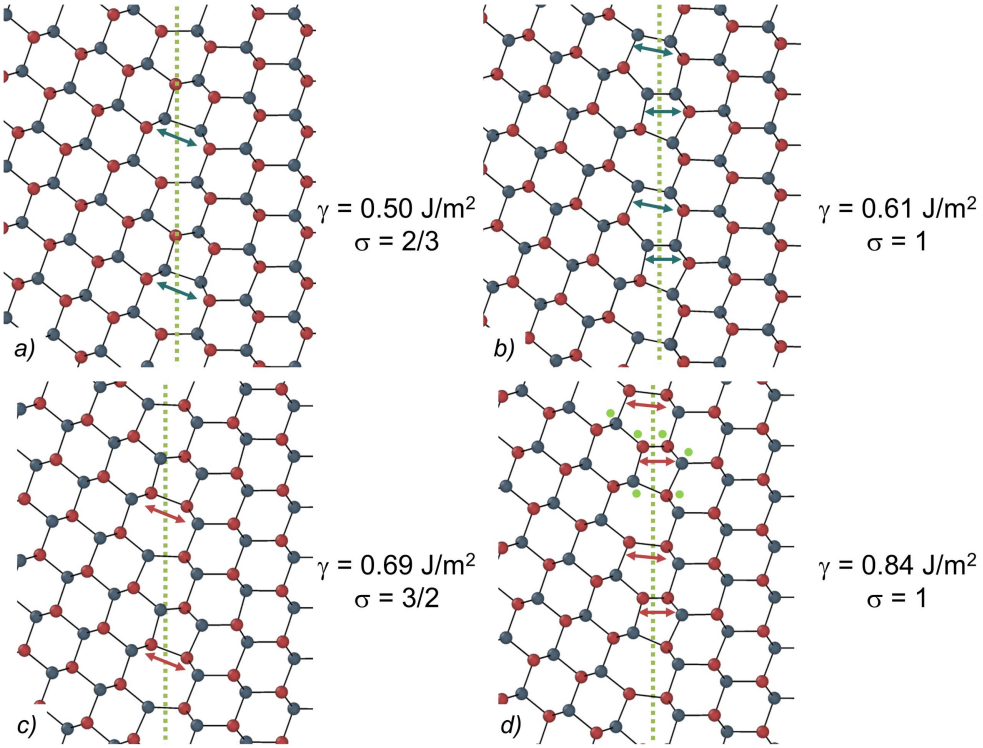

Figure 5. Influence of stoichiometry σ on the GB energy γ of a $\Sigma 3\{111\}\{115\}$ type boundary. Arrows indicate the places of stoichiometric shift. In (d), boundary atoms are marked by an extra green dot close to the atoms with distorted coordination. Cadmium atoms are drawn in red whereas tellurium atoms are blue. Note that bonds are arbitrarily drawn based on the distance between nuclei and not based on actual electronic interactions between atoms.

A comparison between the interface properties of first order, $\Sigma 3$, and second order, $\Sigma 9$, twin boundaries, both with identical interface planes, is displayed in table 4. As could be expected, the energy of the $\Sigma 9$ boundaries is systematically higher than that of $\Sigma 3$ interfaces with the same boundary planes. Nevertheless, the magnitude of this increase strongly varies, depending on the crystallography of the facets considered. Indeed, as displayed in table 4, $\Delta\gamma$ can be as low as $+2\%$ to as high as $+86\%$ in the extreme case of the $\{112\}||\{255\}$ GB. In addition, in this case, the sharp increase in $\Delta\gamma$ is concomitant to a similar increment of the boundary atomic number density difference $\Delta\rho$. Nevertheless, for moderate energy changes, as observed for the $\{111\}||\{115\}$ and $\{110\}||\{110\}$ interfaces, $\Delta\rho$ is actually negative. This means that the extent of the defected area is smaller for the $\Sigma 9$ interface than for its $\Sigma 3$ counterpart, but it also means that the average energy per boundary atom still increases, resulting in a positive value of $\Delta\gamma$. Finally, the interface stoichiometry σ does not seem to show any correlation with the boundary misorientation.

Therefore, considering the four different boundary sets displayed in table 4, it appears that it is hardly possible to infer, *a priori*, the structure and energetics of a $\Sigma 9$ boundary based on the knowledge of a $\Sigma 3$ interface with the same boundary planes. In addition, when combining all facets, the energy range of $\Sigma 9$ interfaces, varying between 0.45 and 0.73 J m^{-2}, overlaps with the one of $\Sigma 3$ interfaces, ranging from 0.35 to 0.68 J m^{-2} as visible in figure 3.

Table 4. GB structural parameters comparison between the Σ3 and Σ9 variants of different sets of GB planes. γ: interface energy, ρ atomic number density, P relative atomic number density and σ Te/Cd ratio.

	γ (J m^{-2})			ρ (u.d.)			P			σ		
	Σ3	Σ9	$\Delta\gamma$	Σ3	Σ9	$\Delta\rho$	Σ3	Σ9	ΔP	Σ3	Σ9	$\Delta\sigma$
{112}||{255}	0.35	0.65	+86%	3.02	3.6	+19%	3.51	4.19	+19%	0.99	1.02	3%
{110}||{114}	0.47	0.73	+55%	3.29	3.75	+14%	2.21	2.52	+14%	0.83	1	+21%
{110}||{110}	0.54	0.63	+17%	3.71	3.6	−3%	1.66	1.61	−3%	1	0.94	−6%
{111}||{115}	0.44	0.45	+2%	3.26	3.25	−0.30%	2.67	2.66	−0.30%	0.75	0.79	+5%

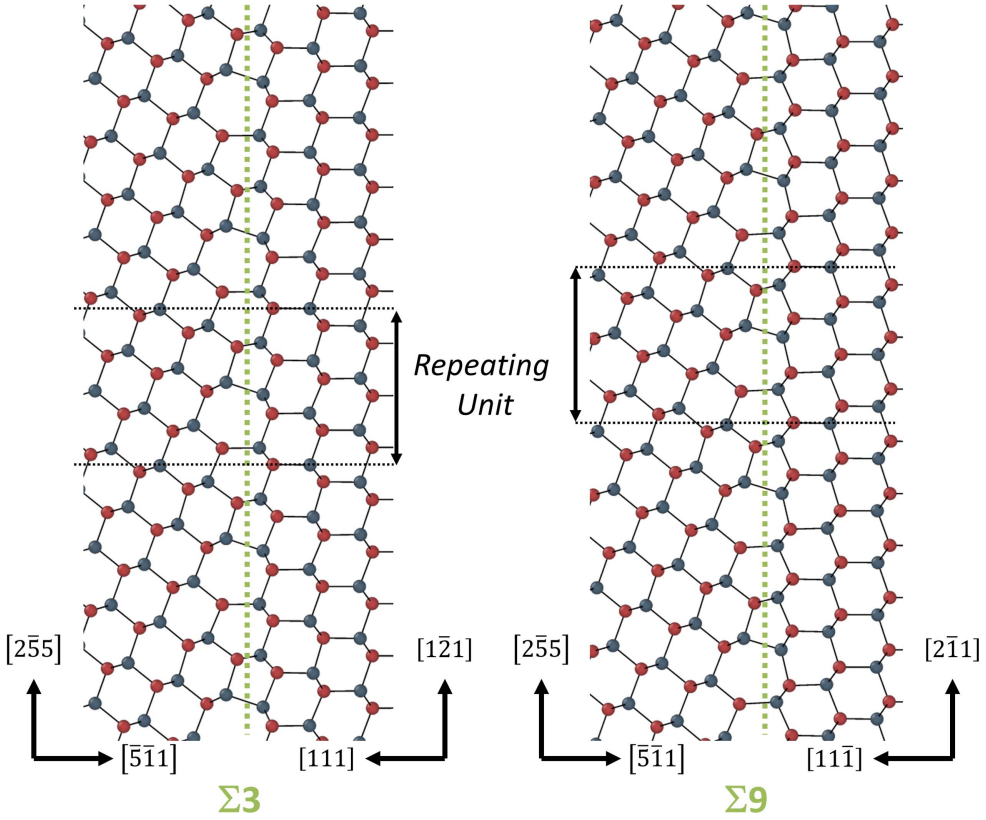

Figure 6. Atomic structure of a $\Sigma3\{111\}\{115\}$ boundary (left) and of the corresponding $\Sigma9\{111\}\{115\}$ interface (right). Cadmium atoms are drawn in red whereas tellurium atoms are displayed in blue. Note that bonds are arbitrarily drawn based on the distance between nuclei and not based on actual electronic interactions between atoms.

As such, when considering the misorientation parameters only, $\Sigma9$ boundaries are not clearly differentiable from incoherent twin boundaries from an energetic point of view. This, once again, stresses the need for full-rotational parameters characterization of GB, when assessing their influence on recrystallization behavior or functional properties.

A special case is observed for the $\{111\}||\{115\}$ interface which exhibits extremely close structural parameters for its $\Sigma3$ and $\Sigma9$ variants. Both structures are presented in figure 6 and they closely resemble each other. This is a particular feature of boundaries composed of a $\{111\}$ interface plane. Indeed, $\Sigma3^n$ type boundaries relate to successive twinning, $\{111\}$ being the twinning plane. Hence, as visible in figure 6, the second order twin can be obtained by taking the $\Sigma3$ variant, fixing the left-hand side of the boundary and performing a pure twist of 180° in the plane of the interface. Therefore, both repeating units present recognizable features and first and second order twins are closely related.

Other Σ *boundaries.* As emphasized in the previous sections, boundary structures are highly dependent on the interface planes considered. Therefore, in order to extract the influence of the Σ value only, it is necessary to compare GB with identical crystallographic planes. This is

Table 5. GB structural parameters of {112}||{112} interfaces with different Σ values.

	Σ3	Σ5	Σ7	Σ11
γ (J m^{-2})	0.53	0.73	0.70	0.78
ρ (u.d.)	2.57	4.07	3.99	3.95
P	1.99	3.16	3.09	3.06
σ	0.60	0.90	0.95	0.94

the case described in table 5 for {112}{112} interfaces with different Σ values ranging from 3 to 11. Due to the lack of boundaries studied, it is not possible to draw any general conclusions regarding interface energy trends with the Σ parameter. Some interesting features can, nevertheless, be noted from table 5. First of all, as mentioned in the previous section, the energy of the Σ3 interface is always lower than their higher Σ counterparts. When comparing the boundary energy of the Σ5 and Σ7 boundaries, it becomes apparent that γ does not simply increase with Σ as could be expected. Indeed, the number density of CSL lattice sites intuitively relates to a notion of ordering, which can naturally be assumed to also exist at the boundary. Nevertheless, although a sharp energy difference is observed between Σ3 boundaries and other misorientations, the energy differences between Σ5, Σ7, and Σ11 are distributed in a much narrower range. As in the previous case, the boundary energy is once again found to increase with the Σ value, whereas the stoichiometry of the boundary does not seem to follow any particular trend. Nevertheless, as mentioned in the case of Σ9 boundaries, when the interface plane is disregarded, it appears that no sharp energetic gap is found to separate Σ3 interfaces from higher-order boundaries. As such, the predominance of the former may primarily relate to their ease of nucleation. In addition, GB mobility may also be invoked as a possible explanation for the low occurrence of these low-energy configurations in the annealed thin films. Indeed, highly coherent sigma GB have practically zero mobility. Therefore, they cannot be easily removed during any competitive and capillary coarsening, leading to their prevalence after heat treatments.

A surprisingly low GB energy is measured in the case of Σ7 {111}||{111} interface (not shown here), with a GB energy of only 0.28 J m^{-2}. This value is even lower than the energy of most stable incoherent Σ3 twin boundaries. This can nevertheless be mitigated by stressing that the energy of symmetric {111} interfaces tends to be underestimated by the BOP, as already previously mentioned in the case of the coherent first order twin.

Conclusions

The structure and energy of CSL boundaries was investigated by mean of MS. As expected, the coherent Σ3 {111}||{111} interface is found to be significantly more stable than any other GB. Nevertheless, when considering other interface planes, a broad spectrum of energies and boundary stoichiometries is observed. Overall, Te-rich boundaries are found to be more energetically stable than their Cd-rich counterparts. This is an important point since Te-rich boundaries are predicted to be less detrimental for the overall cell efficiency upon processing. In addition, symmetric GB tend to exhibit a lower relative atomic number density, indicating a lower degree of relaxation. This, however, does not necessary lead to lower energy configurations, and high-indexed planes can lead to surprisingly stable GB, as it is the case for the Σ3 {112}||{255} interface. In our simulations this is achieved through the formation of a particular dislocation arrangement in the core of the boundary.

For a given set of interface planes, the lowest energy configuration does not simply scale with the Σ value, even though the lowest configuration seems to be always obtained for the Σ3 case. When considering the misorientation solely, i.e. Σ only, a significant overlap in terms of interface energy is found to exist between first order twin boundaries and higher Σ ones. Therefore, we found Σ5, 7 or 9 boundaries with lower interfacial energy than incoherent Σ3 ones formed on other interface planes.

These results stress the shortcoming of GB structure/property correlations, when confining the analysis only to the misorientation space. In addition, the overall predominance of Te-rich CSL, and more detailed knowledge about the magnitude of the stoichiometric shift as a function of the interface crystallography may be useful when interpreting the electronic response of such defects or when designing passivation strategies.

Acknowledgments

The authors acknowledge Nima H Siboni for the fruitful discussions regarding energy calculations and the Max Planck Society for funding this project.

ORCID iDs

Guillaume Stechmann https://orcid.org/0000-0002-6181-9795

References

[1] National Renewable Energy Laboratory 2016 Best research-cell efficiencies http://nrel.gov/ncpv/images/efficiency_chart.jpg
[2] Burst J M *et al* 2016 CdTe solar cells with open-circuit voltage breaking the 1 V barrier *Nat. Energy* **1** 16015
[3] Major J D 2016 Grain boundaries in CdTe thin film solar cells: a review *Semicond. Sci. Technol.* **31** 093001
[4] Visoly-Fisher I, Cohen S R, Ruzin A and Cahen D 2004 How polycrystalline devices can outperform single-crystal ones: thin film CdTe/CdS solar cells *Adv. Mater.* **16** 879–83
[5] Stechmann G *et al* 2017 A correlative investigation of grain boundary crystallography and electronic properties in CdTe thin film solar cells *Sol. Energy Mater. Sol. Cells* **166** 108–20
[6] Ward D K, Zhou X W, Wong B M, Doty F P and Zimmerman J A 2012 Analytical bond-order potential for the Cd–Zn–Te ternary system *Phys. Rev.* B **86** 245203
[7] Ward D K, Zhou X W, Wong B M, Doty F P and Zimmerman J A 2012 Analytical bond-order potential for the cadmium telluride binary system *Phys. Rev.* B **85** 115206
[8] Zhou X W *et al* 2012 High-fidelity simulations of CdTe vapor deposition from a bond-order potential-based molecular dynamics method *Phys. Rev.* B **85** 245302
[9] Zhou X, Ward D K, Wong B M, Doty F P and Zimmerman J A 2012 Molecular dynamics studies of dislocations in CdTe crystals from a new bond order potential *J. Phys. Chem.* C **116** 17563–71
[10] Pauling L 1960 *The Nature of the Chemical Bond* 3rd edn (Ithaca, NY: Cornell University Press)
[11] Coulson C A 1939 The electronic structure of some polyenes and aromatic molecules: VII. Bonds of fractional order by the molecular orbital method *Proc. R. Soc.* A **169** 413–28
[12] Tersoff J 1986 New empirical model for the structural properties of silicon *Phys. Rev. Lett.* **56** 632–5
[13] Tersoff J 1988 Empirical interatomic potential for carbon, with applications to amorphous carbon *Phys. Rev. Lett.* **61** 2879–82
[14] Brenner D W, Shenderova O A, Harrison J A, Stuart S J, Ni B and Sinnott S B 2002 A second-generation reactive empirical bond order (REBO) potential energy expression for hydrocarbons *J. Phys.: Condens. Matter* **14** 783–802

[15] Stechmann G *et al* 2016 Three-dimensional microstructural characterization of CdTe absorber layers from CdTe/CdS thin film solar cells *Sol. Energy Mater. Sol. Cells* **151** 66–80
[16] Plimpton S 1995 Fast parallel algorithms for short-range molecular dynamics *J. Comput. Phys.* **117** 1–19
[17] Ward D K, Zhou X, Wong B M and Doty F P 2013 A refined parameterization of the analytical Cd–Zn–Te bond-order potential *J. Mol. Model.* **19** 5469–77
[18] Stukowski A 2010 Visualization and analysis of atomistic simulation data with OVITO–the Open Visualization Tool *Modelling Simul. Mater. Sci. Eng.* **18** 015012
[19] Maras E, Trushin O, Stukowski A, Ala-Nissila T and Jónsson H 2016 Global transition path search for dislocation formation in Ge on Si(001) *Comput. Phys. Commun.* **205** 13–21
[20] Takeuchi S, Suzuki K, Maeda K and Iwanaga H 1985 Stacking-fault energy of II–VI compounds *Phil. Mag.* A **50** 171–8
[21] Park J-S, Kang J, Yang J-H, Metzger W and Wei S-H 2015 Stability and electronic structure of the low-Σ grain boundaries in CdTe: a density functional study *New J. Phys.* **17** 013027
[22] Stukowski A, Bulatov V V and Arsenlis A 2012 Automated identification and indexing of dislocations in crystal interfaces *Modelling Simul. Mater. Sci. Eng.* **20** 085007
[23] Zhang L, Da Silva J L F, Li J, Yan Y, Gessert T A and Wei S-H 2008 Effect of copassivation of Cl and Cu on CdTe grain boundaries *Phys. Rev. Lett.* **101** 155501
[24] Randle V 2004 Twinning-related grain boundary engineering *Acta Mater.* **52** 4067–81